Physicochemical study of the interaction between gold nanoparticles and lipase from Candida sp. (CALB): Insights into the nano-bio interface

http://dx.doi.org/10.21577/0103-5053.20190127

J. Braz. Chem. Soc., Vol. 30, No. 10, 2231-2242, 2019
Printed in Brazil - ©2019 Sociedade Brasileira de Química

Article

Physicochemical Study of the Interaction between Gold Nanoparticles and Lipase from *Candida* sp. (CALB): Insights into the Nano-Bio Interface

Heloise R. de Barros,[#,a] Mary C. Santos,[a] Leandro R. S. Barbosa,[b] Leandro Piovan[a] and Izabel C. Riegel-Vidotti*[*,a]

[a]*Departamento de Química, Centro Politécnico, Universidade Federal do Paraná (UFPR), 81531-980 Curitiba-PR, Brazil*

[b]*Instituto de Física, Universidade de São Paulo (USP), Cidade Universitária, 05508-090 São Paulo-SP, Brazil*

The surface interactions between gold nanoparticles (AuNPs) and lipase from *Candida antarctica* fraction B (CALB) were investigated at macromolecular and colloidal length-scales. In order to elucidate the reciprocal effect of the interactions on the individual component's properties, CALB was either added during the synthesis of AuNPs or added to pre-synthesized AuNPs. In both cases, it was observed that the AuNPs are spherical and stable and, by fluorescence and circular dichroism spectroscopies, changes were observed in the secondary and tertiary structure of CALB, that were dependent on the AuNPs concentration. Nevertheless, the catalytic activity of CALB was maintained, although at a lower percentage (≥ 80%), thus new bio-functionalities were inserted into AuNPs upon interaction with CALB. Using simple and straightforward approaches and state-of-the-art techniques important knowledge about CALB/AuNPs bioconjugates was gained, thus contributing to the development of new nano-biomaterials and for the safe use of AuNPs in biomedical applications.

Keywords: enzyme, bioconjugate, circular dichroism, fluorescence, catalytic activity, colloids

Introduction

Although in recent years nanotechnology has been successfully applied to the development of new materials with unique properties and many potential applications, the effects of the interactions between nanoparticles and biomolecules, present in the most diverse environments, on the properties of both materials remain poorly understood. The elucidation of the specific interactions involved in the nano-bio interface is fundamental for the safe use of nanomaterials, the manufacturing of nano-bioconjugate structures, the design of new nanomaterials and the evaluation of their biocompatibility or bio adverse effects.[1-4] Thus, an in-depth study on the phenomena that occur at the nano-bio interface not only allows the development of new methodologies, but also contributes to the expansion of possible biological and environmental applications of these materials.[4]

Gold nanoparticles (AuNPs) are of great interest since their properties and synthesis control are well-established as reported by many researchers.[5-7] The surface characteristics, plasmonic properties and high biocompatibility are properties that justify the increasing number of works employing AuNPs in bioapplications.[8-10] Furthermore, AuNPs are attractive because they can be prepared with different morphologies and have their surface modified by simple and straightforward methods employing a huge variety of biomolecules such as amino acids, peptides, proteins, enzymes, deoxyribonucleic acid (DNA) and ribonucleic acid (RNA), among others.[11-14] Based on these reasons and for prospecting new eco-friendly approaches, biomolecules have been used as suitable capping agents for AuNPs.[15-17] Nevertheless, despite the increasing interest in this field, few studies are reported in the literature[16,18-20] using enzymes as the interacting molecules for AuNPs.

Enzymes are remarkable biocatalysts, owing to their chemo-, regio- and stereoselectivity, which are very attractive for a huge range of applications in industry, biotechnology and research.[21-28] Lipase from *Candida antarctica* fraction B (CALB) is widely studied

*e-mail: izabel.riegel@ufpr.br
[#]Current address: Instituto de Química, Universidade de São Paulo (USP), Cidade Universitária, 05508-000 São Paulo-SP, Brazil

and employed since it is an efficient catalyst that can be used for both hydrolysis in aqueous media and esterification in aquo-restricted media or pure organic solvents.[25,29-37]

Different methodologies have been developed in order to alter the stability, activity and even the enantioselectivity of enzymes.[38-43] In this context, the interaction between enzymes and AuNPs can trigger changes in enzyme conformation, and consequently, changes in their inherent properties.[18,20,40,44,45] AuNPs are prone to interact with many biomolecules because of their surface characteristics, however, the effects promoted in the properties of both materials remain poorly understood. Therefore, the understanding of the correlation between the conformation, stability and activity of the enzyme in the presence of nanomaterials is fundamental for biotechnological and biomedical applications of both materials.

To the best of our knowledge, despite the several studies using lipase-AuNP conjugated materials as biocatalysts, biosensors and racemates kinetic resolution,[21,46-49] none of the studies were focused on the specific interactions at the interface of these materials at the molecular and nanoscale levels.

In this work, the interaction between CALB and AuNPs was fully investigated, in terms of the impact of the interaction on the main properties of both the enzyme and the nanomaterial, probed at different length scales using state-of-art techniques. The catalytic activity, the maintenance of bio-functionalities of the enzyme and the morphology and the surface characteristics of the AuNPs were evaluated. Therefore, this work could be used as the basis for further studies that aim to employ enzymes as stabilizing agents for metal nanoparticles or seek to insert bio-functionalities in these nanoparticles. In addition, this study sheds light into the safe use of AuNPs in biological media containing enzymes.

Experimental

Materials

Tetrachloroauric acid ($HAuCl_4.3H_2O$, 30% in dilute HCl, 99.9%) and lipase from *Candida antarctica* fraction B (CALB) (L3170) were purchased from Sigma-Aldrich (São Paulo, Brazil). Sodium borohydride ($NaBH_4$, ≥ 98%) was purchased from Nuclear (São Paulo, Brazil). Tannic acid (Sigma-Aldrich, São Paulo, Brazil), sodium carbonate (Vetec, São Paulo, Brazil) and sodium citrate (Sigma-Aldrich, São Paulo, Brazil) were used as received. Milli-Q grade water (18.2 MΩ cm, Millipore, USA) was used in the preparations for all solutions. Lipase CALB was used without previous purification. For the assays, CALB extract was diluted in water at concentration of 0.1 wt.%, corresponding to 0.42 μmol L^{-1}. The protein concentration of CALB 0.1 wt.% in the dispersion was 14 μg mL^{-1}, determined by Bradford's method.[50]

Synthesis of AuNPs@CALB

The synthesis of citrate-stabilized AuNPs were adapted from a method previously described in the literature.[51] In a typical procedure, the reducing solution was prepared by adding 5 μL of 2.5 mmol L^{-1} tannic acid and 100 μL of 150 mmol L^{-1} Na_2CO_3 to 15 mL of 2.2 mmol L^{-1} sodium citrate fresh solution and kept under magnetic stirring at 70 °C. Subsequently, 100 μL of 25 mmol L^{-1} $HAuCl_4$ was added to the reaction media, immediately changing the color of the dispersion from transparent to purple. The dispersion was kept under magnetic stirring at 70 °C for 10 min. Finally, a dispersion with concentration of 4.4×10^{-9} mol L^{-1} AuNPs was obtained as determined by inductively coupled plasma optical emission spectroscopy (ICP OES). To obtain AuNPs@CALB, 2 mL of CALB 0.1 wt.% was added to 2 mL of previously synthesized citrate-stabilized AuNPs at 2.6×10^{-9} mol L^{-1} kept under magnetic stirring at 25 °C for 30 min to ensure complete adsorption of CALB on the AuNPs surface. The final AuNPs concentration was 1.3×10^{-9} mol L^{-1}.

Synthesis of $_{SA}$CALB/AuNPs

The synthesis of $_{SA}$CALB/AuNP was adapted from a previous method.[52] Into a reaction media containing 1.5 mL of 1.74×10^{-4} mol L^{-1} $HAuCl_4$ and 1.5 mL of water under magnetic stirring at 25 °C, 3.72 mL of CALB 0.1 wt.% was added. Thereafter, 0.72 mL of the reducing agent ice-cold 1.0 mmol L^{-1} $NaBH_4$ was added in one-pot. The color of the dispersion changed rapidly from transparent to purple. The dispersion was kept under magnetic stirring at 25 °C for 30 min to ensure complete reaction. The final AuNPs concentration was 1.0×10^{-9} mol L^{-1}, as determined by ICP OES.

Characterization techniques

Transmission electron microscopy (TEM)

Transmission electron microscopy (TEM) (JEOL 1200EX-II microscope) was performed at an acceleration voltage of 120 kV in Electron Microscopy Centre (CME-UFPR). A drop (ca. 3 μL) of the sample was placed on lacey carbon-coated grids and embedded in a matrix of 1-ethyl-3-methylimidazolium tetra-fluoroborate (ionic liquid EMI-BF4) (Sigma-Aldrich, São Paulo,

Brazil), the excess was removed with filter paper and allowed to air-dry. High resolution TEM (HR-TEM) was performed at 200 kV (JEOL 2100 TEM-FEG microscope) at the Brazilian Nanotechnology National Laboratory (LNNano-CNPEM). The size and size distribution of the nanoparticles were determined using ImageJ software.[53]

Inductively coupled plasma optical emission spectroscopy (ICP OES)

The final concentration of gold was determined by ICP OES (Thermoscientific iCAP 6000 series ICP spectrometer). The calculation of AuNPs was determined according to a previously described methodology.[54] Firstly, the volume of one nanoparticle was determined by the definition $V = 4 / 3\pi R^3$ using the radius (R) of AuNPs previously determined by TEM. Then, by using the density of gold (19300 kg m^{-3}), Avogadro's number (6.022×10^{23} particles) and the concentration (in mg L^{-1}) determined by ICP OES measurements, the molar concentration of AuNPs dispersion was obtained.

UV-Vis spectroscopy

UV-Vis spectroscopy (UV-Vis Agilent 8453) was used to characterize AuNP samples by the surface plasmon resonance (SPR) band with a maximum wavelength (λ_{max}) at around 510-530 nm in a quartz cuvette of 10 mm of optical path.

Steady-state fluorescence spectroscopy

Tryptophan fluorescence measurements were performed in a Cary Eclipse Fluorescence Spectrophotometer (Varian). Samples were excited at 295 nm and the emission spectra recorded in the range from 305 to 500 nm at 5 nm bandwidth for both emission and excitation, using a 4 × 10 mm (excitation × emission) quartz cuvette of 1 cm optical path length. As AuNPs can increase the turbidity of CALB dispersions, the fluorescence intensities of every spectra were corrected by taking into account the inner filter correction using the following equation:[55]

$$F = F_0 10^{(A_{ex} l_{ex})} 10^{(A_{em} l_{em})} \quad (1)$$

where, F and F_0 are the corrected and the measured fluorescence intensities, respectively; A_{ex} and A_{em} are the measured absorbances acquired at λ of excitation and emission, respectively; l_{ex} and l_{em} are the optical path lengths of the cuvette in cm. In this study, the following values were used for the inner filter correction: A_{ex} = 295 nm, A_{em} = 305-500 nm, l_{ex} = 0.2 cm and l_{em} = 0.5 cm. The values of fluorescence were obtained by the integration of the fluorescence peak area in the range of 320-380 nm.

Circular dichroism (CD) spectroscopy

Circular dichroism (CD) spectroscopy (Jasco J-815 Spectrometer) was performed ranging from 195 to 260 nm with scanning speed of 50 nm min^{-1}, bandwidth of 1 nm, data pitch of 0.5 nm, using a quartz cell of 1 mm at 25 °C controlled by a Peltier system. All measurements were recorded by an average of 10 accumulations and the CD spectra were corrected by the water spectrum. The spectra were displayed using the molar residue ellipticity (MRE) deg cm^2 $dmol^{-1}$ using the following relation:

$$MRE = \frac{MRW\theta}{10dC} \quad (2)$$

where, θ is the ellipticity in degrees, d is the path length of the cell in centimeters and C is the concentration of protein in g mL^{-1}. MRW is the mean residue weight and is defined as MRW = M / (N – 1), where M is the molecular mass in Daltons and N is the number of amino acids of the protein. For CALB, the value of M is 33.000 g mol^{-1} and N is 317.[56]

Size exclusion chromatography (SEC)

Size-exclusion chromatography (SEC) coupled with multidetector analyses were performed to determine the weight average molar mass $\overline{M}_w$, and polydispersity (PD = $\overline{M}_w$ / $\overline{M}_n$, $\overline{M}_n$ is the number average molecular weight) of the samples, on a Waters model 2410, equipped with four columns (Ultrahydrogel 2000, 500, 250 and 120, Milford, MA, USA). The columns were serially connected to the multi detection system consisting of a Waters 2410 differential refractometer (RI) detector (Milford, MA, USA), and a DSP-F Wyatt Technology multiangle laser light scattering (MALLS) detector (Santa Barbara, CA, USA). $NaNO_2$ (0.1 mol L^{-1}) containing NaN_3 (0.5 g L^{-1}) was used as the eluent at a flow rate of 0.6 mL min^{-1}. The sample was dispersed in the eluent at a concentration of 2.0 mg mL^{-1}, and filtered (0.45 μm, cellulose acetate filters, Millipore).

Zeta potential

Zeta potential measurements were obtained (Malvern Zetasizer Nano ZS90, using a disposable folded capillary cell DTS 1070, Malvern Instruments) by the electrophoretic mobility (U_E) and converted to the zeta potential value by Henry's equation:

$$U_E = \frac{2\varepsilon\zeta f(ka)}{3\eta} \quad (3)$$

where, ε is the dielectric constant, ζ is the zeta potential (in mV), η is the viscosity and f(ka) is the Henry function, which is calculated from the Smoluchowski approximation

(f(ka) = 1.5).[57] Zeta potential values are the average of five measurements.

Small angle X-ray scattering (SAXS)

Small angle X-ray scattering (SAXS) data were collected on the laboratory-based SAXS equipment Xenocs XEUSS™, at the Institute of Physics, University of São Paulo. The radiation was generated by a GENIX™ source (Cu K_α edge, $\lambda = 1.54$ Å) with the beam focused by FOX2D™ optics. The beam collimation was performed by two sets of scatterless slits (Xenocs 2.0). In the high flux mode, the flux was ca. 1×10^8 photons s^{-1} with a beam size of 1×1 mm^2. The 2D SAXS data were collected with a Dectris Pilatus™ 300k detector. Liquid dispersion samples were filled into quartz capillaries with 1.5 mm in diameter. For SAXS measurements, the distance from sample to detector was set to 0.9 m, giving a q range of $0.11 < q < 0.40$ $Å^{-1}$ where q is the reciprocal space-momentum transfer modulus defined as $q = (4 \sin\theta) / \lambda$ with 2θ the scattering angle and λ as the radiation wavelength. Several frames for 1800 s were measured in order to check for radiation damage to the sample as well as to average and increase the signal-to-noise ratio. Data treatment were performed using python scripts with PyFy libraries for the integration of the 2D data.

Additional measurements were also taken in the Brazilian National Synchrotron Light Source, LNLS, Campinas, SP. In this case the used q range was quite similar $0.11 < q < 0.50$ $Å^{-1}$, being the sample to detector distance ca. 1000 mm and the detector was a PILATUS 300K.

The scattered intensity, I(q), for an isotropic system of monodisperse spheres in a small angle X-ray scattering (SAXS) experiment can be expressed as:[58,59]

$$I(q) = kn_pP(q)S(q) \quad (4)$$

where n_p is the particle number density and k is a constant that depends only on instrumental characteristics, P(q) is the particle form factor, whereas S(q) is the interparticle structure factor and for non-interacting systems can be treated as S(q) ca. 1.

An interesting function that provides structural information about the scattering particles is the well-known pair distance distribution function, p(r). In the absence of interference effects, a Fourier transform connects P(q); and hence I(q), to the p(r) function, which is interpreted as the probability of finding a pair of small scattering elements inside the scattering particle, this function can be written as:[60]

$$p(r) = \frac{1}{2\pi^2}\int_0^\infty I(q)qr\sin(qr)dq \quad (5)$$

This function also provides information about the shape of the scattering particles as well as its maximum dimension, D_{max}, accounted for a certain r value where p(r) tends to zero. For spheres, p(r) is symmetrically shaped (bell-like shape) with peak position around the radius of the scattering particle.[59] Moreover, it is also possible to infer about partial scattering due to particle aggregation using the p(r), as shown in previous studies.[61]

Enzymatic activity

Enzymatic activity assays were adapted from a previous work.[50] The enzymatic hydrolysis of 4-nitrophenyl palmitate (*p*NPP) was monitored by the appearance of the product *p*-nitrophenolate (*p*NP) (Scheme 1), using a UV-Vis Spectrophotometer (Shimadzu UV PC2501). In a typical procedure, 0.5 mmol L^{-1} of *p*NPP solution was prepared in isopropanol. In a 1 cm path length quartz cuvette containing 2.6 mL of phosphate buffered saline (PBS) (140 mmol L^{-1} NaCl, 27 mmol L^{-1} KCl, 10 mmol L^{-1} phosphate buffer; pH 7), 0.2 mL of *p*NPP solution was added and homogenized. Then, 0.2 mL of the sample was added, and the solution was homogenized once again. The hydrolysis product *p*NP was monitored by the absorbance at $\lambda = 405$ nm. Data were collected from 20 spectra, ranging from $\lambda = 210$-500 nm, with 2 nm of data interval and scan speed of 480 nm min^{-1} for 25 min, at 37 °C. The *p*NP concentration was determined by Lambert-Beer law using 8030 L mol^{-1} cm^{-1} as the extinction coefficient.[62]

Results and Discussion

Morphology, size and stability of $_{SA}$CALB/AuNPs and AuNPs@CALB

The main investigated properties, evidencing the stability of the particles, were size and size distribution.

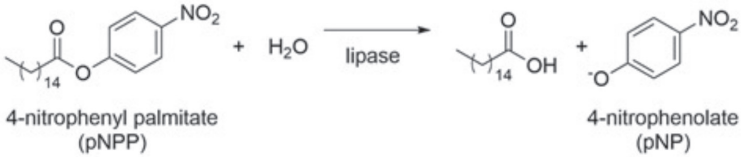

Scheme 1. Enzymatic hydrolysis of 4-nitrophenyl palmitate (*p*NPP). The product *p*-nitrophenolate (*p*NP) was monitored by UV-Vis spectroscopy at $\lambda = 405$ nm.

It is worth mentioning that CALB alone was not able to reduce $AuCl_4^-$ in order to produce nanoparticles under the same reaction conditions. However, when using $NaBH_4$ as the reducing agent for $AuCl_4^-$, CALB exhibited great performance as a stabilizing agent (SA) in the formation of homogenous and stable AuNPs. The as-prepared bio-hybrid material is referred as $_{SA}$CALB/AuNPs. In addition, it is well known that the synthesis of AuNPs in absence of any stabilizing agents (by bottom up synthesis approaches) leads to nanoparticle aggregation and consequently to the loss of AuNPs inherent properties.[52] Therefore, CALB is a promising capping agent for both controlling the size and morphology of AuNPs as well for introducing bio-functionalities to nanomaterials.

In addition, in order to elucidate the source of interaction between CALB and AuNPs, another approach adding CALB to a previously synthesized AuNPs was designed for comparison. For this, citrate-stabilized AuNPs were prepared since it is a well-stablished methodology for obtaining stable AuNPs with size and morphology control.[51,63,64] Moreover, as AuNPs' properties highly depend on their size,[65] AuNPs with approximately the same size as $_{SA}$CALB/AuNPs were synthesized for effective comparison. Then, the bio-hybrid material, referred as AuNPs@CALB, was successfully prepared.

UV-Vis spectroscopy was used to monitor the SPR band of both materials (Figure 1). The SPR band is sensitive to the nanoparticles' properties, since it is a result of the interaction between an incident electromagnetic radiation and the gold surface free electrons (outer shell and conduction-band). These electrons oscillate collectively absorbing energy and thus producing the SPR band that depends on the changes of polarization in the electronic cloud surrounding AuNPs' surfaces. Because of this, the different sizes, morphology, dispersion media, dielectric constant, pH and interaction with other molecules, among others, will promote modifications of the charge distribution density on AuNPs' surfaces, and consequently, on the collective oscillation of electrons.[66,67] Therefore, the SPR band is a useful tool to characterize changes on AuNPs regarding size, shape, morphology and changes on nanoparticle surfaces.[66] Citrate-stabilized AuNPs presented an absorption maximum (λ_{max}) of 510 nm at UV-Vis spectrum. The shift to higher λ_{max} (515 and 524 nm for AuNPs@CALB and $_{SA}$CALB/AuNPs, respectively), confirmed the adsorption of CALB on AuNPs' surfaces due the changes promoted in the electronic distribution on AuNPs' surfaces. Furthermore, the λ_{max} shift and the broader SPR band for $_{SA}$CALB/AuNPs suggested that the adsorption of CALB on AuNPs occurred differently for AuNP@CALB and $_{SA}$CALB/AuNPs. It is worth mentioning that AuNPs@CALB and $_{SA}$CALB/AuNPs were also evaluated in phosphate buffer solution at pH 6.8 and the corresponding SPR band (maximum absorption and shape) was monitored over 24 h to verify the stability of the samples. The samples remained stable as presented in the Supplementary Information (SI) section (Figure S1).

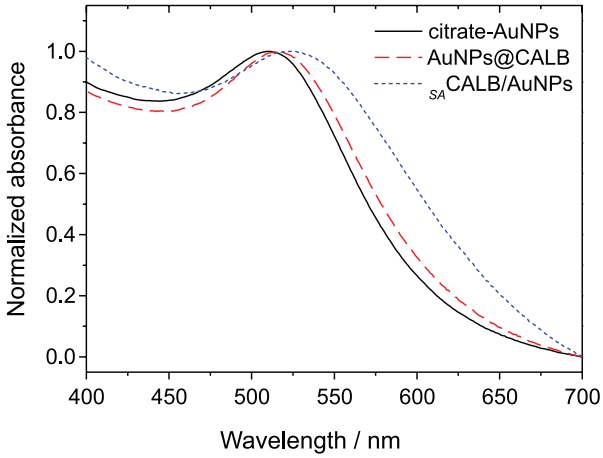

Figure 1. SPR band at the UV-Vis spectrum of the citrate-stabilized AuNPs, AuNPs@CALB and $_{SA}$CALB/AuNPs, clearly showing the shift to higher λ_{max} due to the CALB adsorption on AuNPs surface. The spectra were normalized for the comparison of the λ_{max} shifts.

TEM images confirmed the homogenous size of $_{SA}$CALB/AuNPs with an average size of 3.5 ± 0.7 nm (Figure 2). It was observed that AuNPs were surrounded by the suggested structure of CALB (Figure 2a). By HR-TEM, a thin layer of CALB surrounding the AuNP was observed (inset in Figure 2a). In addition, Figure 2b shows the CALB dispersion (in the absence of AuNPs) evidencing the globular aggregates of the enzyme.

Figure 2c shows the TEM image of citrate-stabilized AuNPs with an average size of 4.3 ± 0.7 nm. Figure 2d shows AuNPs@CALB, which have the same average size

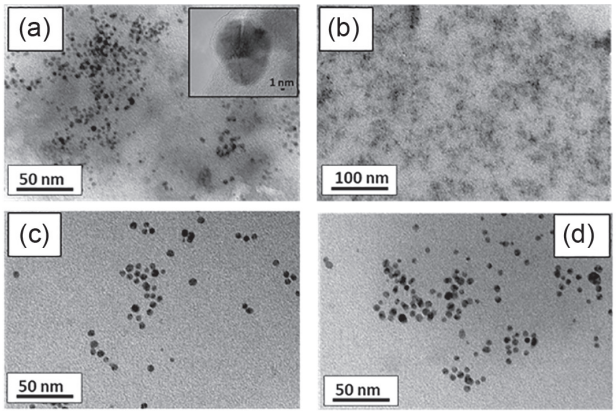

Figure 2. TEM images of (a) $_{SA}$CALB/AuNPs, the inset image, acquired by HR-TEM, clearly shows a layer of CALB on AuNP surface, (b) CALB dispersion, (c) citrate-stabilized AuNPs and (d) AuNPs@CALB.

of the citrate-stabilized AuNPs. Hence, as seen by the TEM images, the addition of CALB to the AuNPs did not induce nanoparticle's aggregation.

In order to get more information regarding the nanoparticle's morphological properties and their interaction with CALB, small angle X-ray scattering was used. Figure 3 shows the SAXS curves of citrate-stabilized AuNPs (a) and AuNPs@CALB (b) of CALB. The inset of each figure displays the respective p(r).

As can be seen in Figure 3, the scattering curves in the absence and the presence of CALB are quite similar and resemble those from small spherical scattering particles in solution.[52]

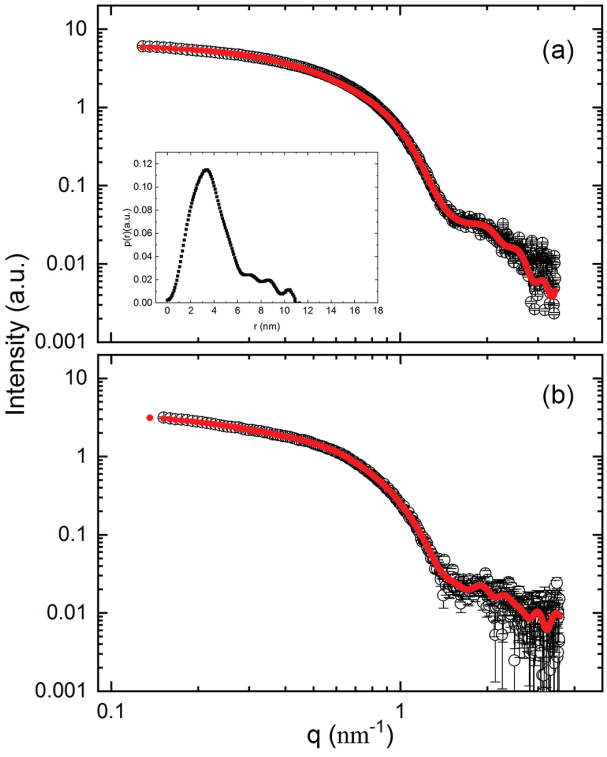

Figure 3. Small angle X-ray scattering curves of citrate-AuNPs (a) and AuNPs@CALB (b). The black open circles and the solid line represent the experimental data points and the theoretical fitting curve, respectively.

A representative p(r) function can be observed in the inset of Figure 3a. As one can see, the p(r) function is symmetrical (bell-like profile) up to r ca. 6 nm. Interestingly, in both cases, the maximum frequencies occurs at ca. 3.0-3.5 nm, in very good agreement with TEM micrographics. Noteworthy, the value of D_{max} (ca. 12 nm) is quite large when compared to the value corresponding to the maximum of frequencies (ca. 3.5 nm). Such a fact reflects that there is a not neglectable partial particle aggregation in the system or even a partial clustering, which was not evident in the TEM images. It should be stressed that there is a quite important difference in the number of nanoparticles probed at the same time when comparing both techniques (TEM *vs*. SAXS). SAXS probes a determined scattering volume that contains a much larger number of objects when compared to TEM observation. The difference in particle concentration can be the explanation for this partial aggregation.

Thus, using two complementary techniques, the citrate-AuNPs and AuNPs@CALB were considered comparable in size and morphology and suited for the comparative studies of the physicochemical interactions between AuNPs and CALB.

The interaction between proteins and metallic nanoparticles is attributed to the preferential interaction of the amino acid residues from proteins onto nanocrystal facets.[15] It was proposed that this interaction pattern is followed by the anchoring, crawling and further binding of the biomolecule on the nanocrystals.[15,68] As observed by TEM images, these interactions do not have impact on the AuNP's size and morphology but induces changes in the SPR band. Therefore, to further elucidate the interactions and their influence on the physicochemical properties of the hybrid materials, the reciprocal effects of the interactions on the individual components (AuNPs and CALB) were investigated.

Spectroscopic properties of CALB in the samples $_{SA}$CALB/AuNPs and AuNPs@CALB

The maintenance of the tertiary structure of CALB was monitored by the intrinsic tryptophan (Trp) fluorescence (Figure 4a). CALB structure has five Trp residues on its sequence of 317 amino acids that provide a sensitive tool to investigate changes at CALB conformation through the interaction with AuNPs.[56] CALB exhibited a fluorescence maximum at 323 nm that is typical for buried Trp residues in enzyme structures.[69] Nonetheless, in the presence of AuNPs, the Trp fluorescence spectra presented a red shift to 349 and 351 nm for AuNPs@CALB and $_{SA}$CALB/AuNPs, respectively. The bathochromic shifts pointed out that Trp residues are exposed to a more polar environment, indicating an interaction between CALB and AuNPs.[70] Hence, the interaction of CALB with AuNP surfaces and during the AuNPs' growth, caused changes in the tertiary structure of CALB or around some of the Trp residues of the polypeptide chain.

As Trp residues are quite hydrophobic, the interaction with AuNPs could lead to the exposure of these residues to the aqueous media.[70] In addition, it is well-known that this change in protein conformation might cause their unfolding, and consequently, the decrease or even the loss of their inherent properties.[71] To further elucidate

the CALB's properties and to correlate with the results observed by fluorescence, CD spectroscopy was performed in order to monitor changes of secondary structure of CALB due to AuNP interactions (Figure 4b).

CALB chains fold into an α-helix, which is characterized by the two negative peaks at 208 and 222 nm in the CD spectra.[56] Interestingly, despite the distinct spectra observed for Trp fluorescence, the CD spectra of AuNPs@CALB and CALB are very similar. The signal at 222 nm, characteristic of α-helical proteins remained unchanged, indicating that an order-disorder (unfolding) process[72] has not occurred. On the other hand, for $_{SA}$CALB/AuNP the intensity of the signals at 208 and 222 nm were slightly reduced. The decrease in the CD ellipticity is associated with CALB aggregation.[56] Although the spectrum kept the same typical profile and no new signals were observed for $_{SA}$CALB/AuNPs, the result suggests a decrease in CALB α-helix content or a partial conversion to a coil structure.[73] Therefore, neither AuNPs@CALB nor $_{SA}$CALB/AuNP displayed significant loss of their secondary structure. When comparing both samples, adding CALB to pre-synthesized AuNPs (AuNPs@CALB) leads to less influence on CALB secondary structure. It is reasonable to infer that since CALB was present in all steps during AuNP synthesis to build up $_{SA}$CALB/AuNPs, this could have caused changes in CALB secondary structure.

It is worth emphasizing that these findings cannot be associated with any reaction between $NaBH_4$ (used for AuNP synthesis) and enzyme, since as a weak reducing agent, $NaBH_4$ is not able to reduce the functional groups of CALB's structure or damage CALB's structure in any way. Under those same reaction conditions, $NaBH_4$ is able to reduce only aldehydes and ketones, not present in CALB's structure.[74] Thereupon, the changes in CALB conformation are dependent on the selected methodology to produce bio-hybrid materials.

Catalytic activity of CALB in the samples $_{SA}$CALB/AuNPs and AuNPs@CALB

In order to evaluate whether the structural changes suffered by CALB, due to the interaction with AuNP, were able to alter the enzyme activity, the enzymatic activity, i.e., the hydrolysis of 4-nitrophenyl palmitate (*p*NPP) (Figure 5), were carried out. In the absence of AuNP, CALB quickly catalyzes the *p*NPP hydrolysis, obtaining the 4-nitrophenolate (*p*NP) as product and characterized by the yellow color that was recorded at λ = 405 nm in a UV-Vis spectrum (circle symbol, Figure 5). The same reaction, in the absence of any catalyst, importantly reduced *p*NPP auto-hydrolysis at the same period (star symbol, Figure 5). As expected, based on the outcomes obtained from Trp fluorescence and CD spectroscopies, AuNPs@CALB and $_{SA}$CALB/AuNP exhibited reduced catalytic activity when compared to CALB (triangle and square symbol, respectively, Figure 5). The catalytic activity of CALB in AuNPs@CALB was slightly higher than in $_{SA}$CALB/AuNPs, in agreement with the CD spectra findings. Despite the standard deviation (SD) being very similar for both samples, the standard error (SE) of the average (red bars) showed low variation in relation to the SD since SE values provide the uncertainty of the measurements around the estimate average.[75] Therefore, the relation between SD and SE indicates that the measurements are accurate, confirming the slight increase of the catalytic activity of AuNPs@CALB in relation to $_{SA}$CALB/AuNPs.

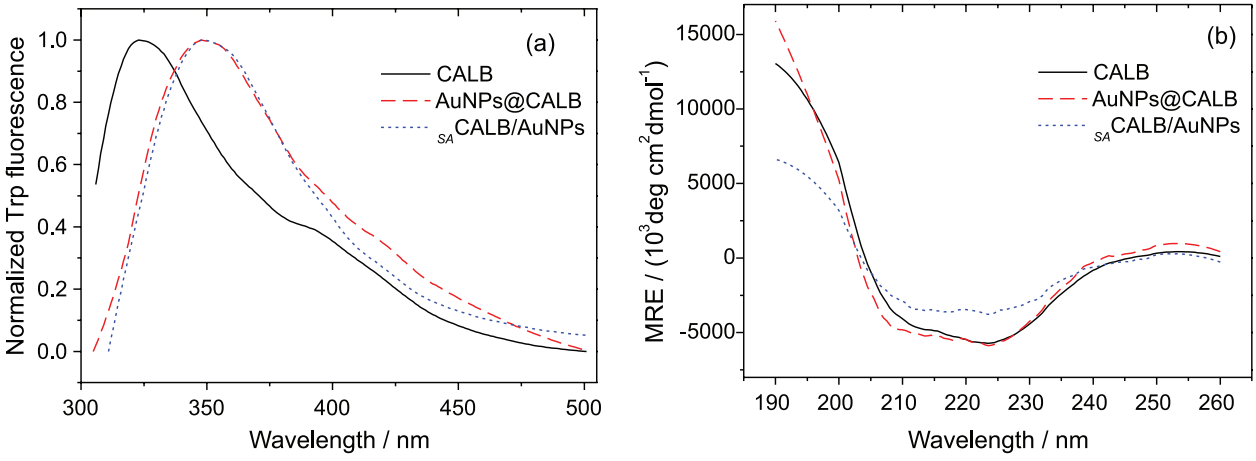

Figure 4. CALB in the absence (black lines) and presence of AuNPs@CALB (red lines) and $_{SA}$CALB/AuNPs (blue lines) characterized by (a) Trp fluorescence and (b) CD spectroscopy. The Trp fluorescence intensity spectra were normalized with respect to the corresponding λ_{max} of the SPR band. CD spectra were corrected by subtraction of the blank spectra and displayed in units of MRE.

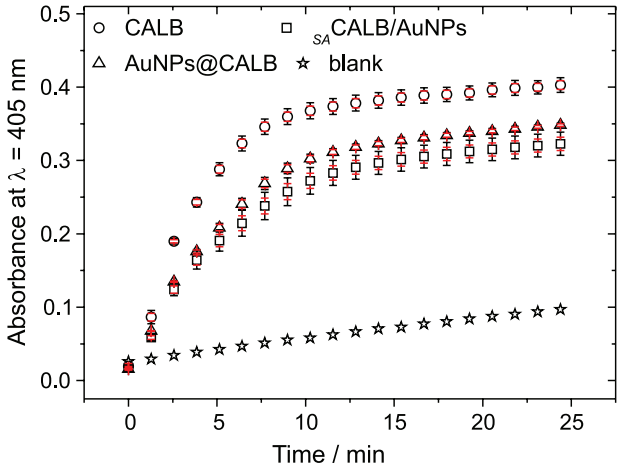

Figure 5. Formation of 4-nitrophenolate (*p*NP), monitored at λ = 405 nm by UV-Vis absorption, from the hydrolysis of 4-nitrophenyl palmitate (*p*NPP) in the presence of CALB (circles), AuNPs@CALB (triangles) and $_{SA}$CALB/AuNPs (squares). The blank represents the control of pNPP auto-hydrolysis (in the absence of any catalyst). The black bars indicate the SD and the red bars indicate the SE of the average of 3 measurements.

The retention of the relative catalytic activity was 87 and 80% for AuNPs@CALB and $_{SA}$CALB/AuNPs, respectively, in comparison to the catalytic activity of CALB. Moreover, the amount of the product formed for AuNPs@CALB and $_{SA}$CALB/AuNPs were 72 and 70%, respectively, higher in comparison to the activity in the absence of any catalyst (*p*NPP auto-hydrolysis). Then, by the outcomes from catalytic activity assays, it was evidenced that the interactions between CALB and AuNPs maintained the catalytic properties of CALB, although at a lower percentage.

Therefore, the time course study of the catalytic activity reinforced the results from Trp fluorescence and CD. The interaction between CALB and AuNPs is evident and led to changes in the conformation of CALB; however, with no expressive loss of the catalytic activity. In that way, as seen by Trp fluorescence, the tertiary structure of CALB changed both in AuNPs@CALB and in $_{SA}$CALB/AuNPs, and probably in a very similar way, as seen by the very close value of the λ_{max} fluorescence shift. However, looking at the secondary structure, the alterations of CALB conformation in $_{SA}$CALB/AuNPs were more pronounced than in AuNPs@CALB, further confirmed by the reduction of the catalytic activity of the former.

Probing the AuNPs/CALB interactions at macromolecular and colloidal length-scales

In order to deeply understand the differences in the hybrid material's properties, zeta potential measurements were done to explore the affinity between the enzyme and the nanoparticles (Figure 6).[76] The zeta potential (ζ) determination is a suitable technique for the assessment of the colloidal stability which plays a central role in the *in vivo* application of this system.[77] The ζ of citrate-stabilized AuNPs was −48.4 ± 2.6 mV. This value is indicative of the high stability of the particles. The negative charge arises from the citrate ions on the AuNPs surface.[78] The ζ of CALB was −5.3 ± 0.1 mV and the values of AuNPs@CALB and $_{SA}$CALB/AuNPs were −27.9 ± 1.8 and −17.5 ± 2.4 mV, respectively. The enhancement of the negative character of the bioconjugates surface charge demonstrates the increase in the colloidal stability of these systems and is a fingerprint of protein adsorption leading to a decrease in the overall electrostatic potential. These findings are in quite good agreement with SAXS measurements, where a higher tendency of aggregation was observed when the AuNPs were in the presence of CALB (see Figure 3).

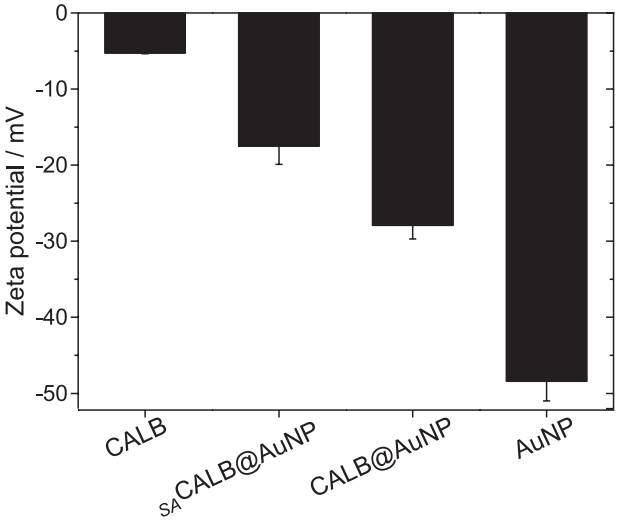

Figure 6. Zeta potential values (ζ) of CALB, $_{SA}$CALB/AuNPs, AuNPs@CALB and citrate-stabilized AuNPs.

Moreover, this behavior indicates the favorable interactions between the constituents of the bio-hybrid material, mainly through electrostatic interactions. It is widely known that the enzymes and metallic nanoparticles' favorable interactions arise from thiolated amino acids.[79-81] With respect to that, CALB has in its structure four methionine and six cysteine residues highly favoring its interaction with AuNPs.[48,52,75,82,83] Besides, the more negative zeta potential value for AuNPs@CALB suggests superior stability in relation to $_{SA}$CALB/AuNPs, since the increase of repulsive forces reduces the tendency of colloidal aggregation.[77] The zeta potential experiments confirmed that CALB adsorption took place on AuNPs surfaces for both AuNPs@CALB and $_{SA}$CALB/AuNPs.[84] The adsorption was also confirmed by SDS page (Figure S2,

SI section). The characteristic band at 33 KDa of CALB is clear, whereas in the presence of AuNPs no protein fraction was noticed. It was also observed, that the CALB/AuNPs interactions protects CALB against severe denaturation (SDS page, SI section).

In addition, via size exclusion chromatography (SEC, Figure 7) it was observed that the retention volume of the hybrid materials is lower than the retention volume of CALB. This indicates that these materials do not interact with the column as efficiently as CALB, indicating their higher hydrodynamic volumes. Therefore, the association of SEC and SDS-PAGE analyses confirmed that the interaction between AuNPs and CALB promotes a complex structural arrangement that is higher in size than free CALB.

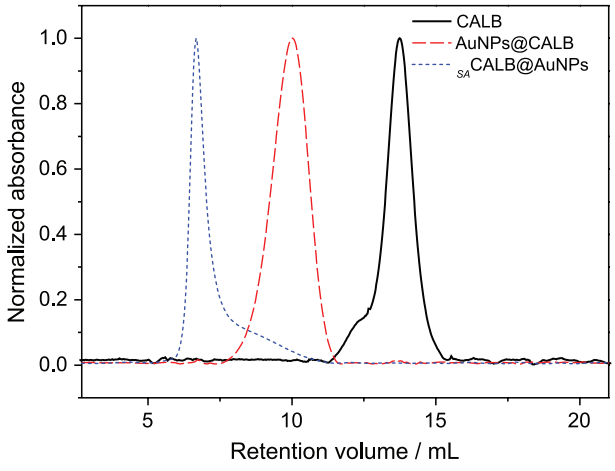

Figure 7. SEC chromatogram of CALB, AuNPs@CALB and $_{SA}$CALB/AuNP in phosphate buffer at pH 7, clearly showing the lower retention volume of CALB when in the presence of AuNPs.

Finally, associating with CD conclusions, the zeta potential confirmed that colloidal aggregation is more likely to occur in $_{SA}$CALB/AuNPs than in AuNPs@CALB. In addition, taking into account that the theoretical isoelectric point (pI) of CALB is 5.8[56] and that the aqueous media's pH ca. 5.5, instability of CALB is expected in aqueous media. This being so, the interaction of CALB and AuNPs is a way to increase the enzyme's stability in water, as in AuNP@CALB and $_{SA}$CALB/AuNPs, also maintaining its important properties such as catalytic activity.

In order to further analyze the AuNPs@CALB's properties, the effect of crescent AuNP:CALB ratios on the spectroscopic properties of CALB was explored. Toward this goal, aliquots of citrate-stabilized AuNPs were added dropwise into CALB dispersion and further investigated by fluorescence spectroscopy.

Upon the addition of AuNPs to the CALB dispersion, the Trp fluorescence intensity continuously decreased (Figure 8). This pattern relied on the quenching effect that can be promoted by the solvent molecules close to the Trp residues or by the neighboring groups present in protein structure.[70] Then, the decrease of fluorescence intensity can be associated with the interaction between CALB and AuNPs.[85] In addition, zeta potential values were also determined to confirm the interaction between CALB and AuNPs. The values of zeta potential changed from approximately −5 to −34 mV with the addition of the AuNPs. The increasing of the negativity of the zeta potential at each aliquot indicated the adsorption of CALB on AuNPs surface, possibly by means of the thiolate amino acid residues, and, at the same time, enhancing the colloidal stability of the system.[82]

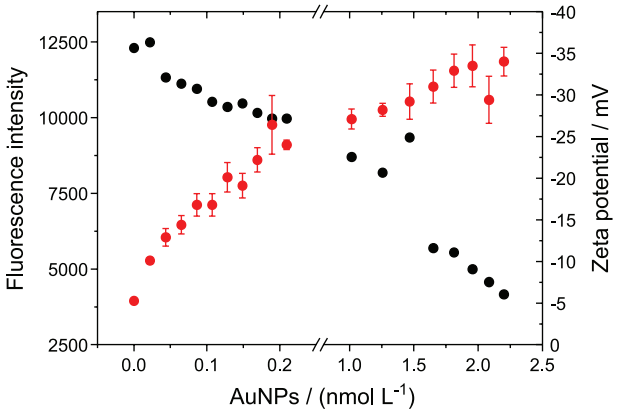

Figure 8. Changes of fluorescence intensity (black circles) and zeta potential values (red circles) upon increasing the AuNPs content on CALB dispersion, initially at 0.42 μmol L^{-1}. The fluorescence intensities of each spectra were corrected by the inner filter effect.

Figure 9 shows the Trp fluorescence bathochromic shift upon AuNP addition. The Trp fluorescence λ_{max} increased according to the increase of AuNP concentration (C_{AuNPs}). The λ_{max} = 323 nm for C_{AuNPs} = 0 changed to 340 nm at C_{AuNPs} = 2.2 nmol L^{-1} (maximum concentration). The magnitude of the Trp fluorescence λ_{max} shift is related to neighboring molecules such as solvent molecules or other molecules surrounding the Trp residues exposed to the media.[70] Therefore, the presence of AuNPs promoted changes of CALB conformation leading to the exposition of Trp residues to the media. Yet, the exposition of Trp residues is dependent on the AuNP concentration, since at C_{AuNPs} = 1.6 nmol L^{-1} (pink line) these changes became even more expressive.

Both, fluorescence intensity and Trp λ_{max}, are very sensitive to conformational changes of CALB.[69] The decrease of the emitted fluorescence intensity without red shift in the λ_{max} can be interpreted as an interaction between CALB and AuNP, without significant changes in the Trp' surroundings polarity,[82] despite such a proximity

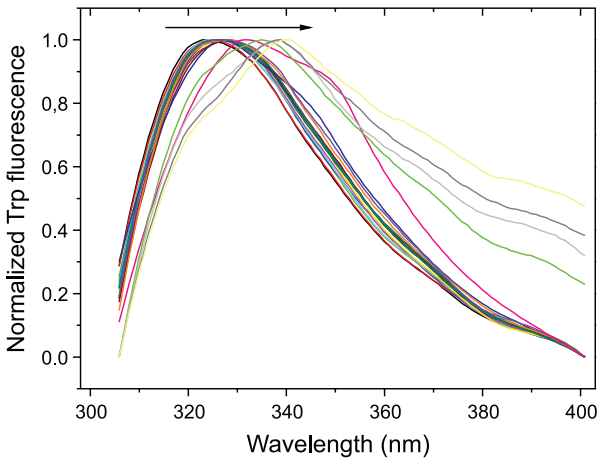

Figure 9. Normalized Trp fluorescence bathochromic shifts as a function of the increasing AuNPs content from C_{AuNPs} = 0 to 2.2 nmol L^{-1} on CALB dispersion initially at 0.42 µmol L^{-1}.

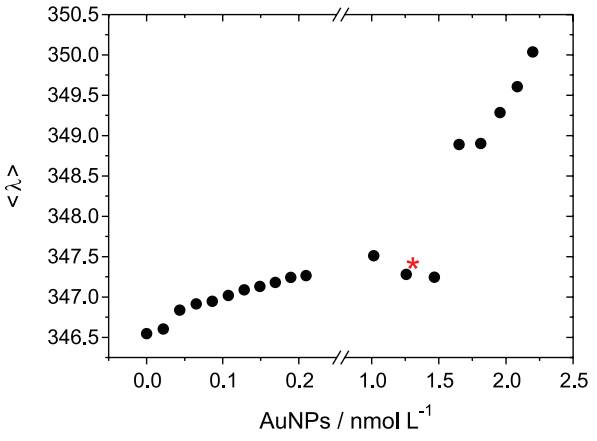

Figure 10. Spectral center of mass (<λ>) as a function of the increasing AuNPs content on CALB dispersion initially at 0.42 µmol L^{-1}. The red star represents <λ> for the sample AuNPs@CALB.

being evidenced by fluorescence quenching. Conversely, changes in both the intensity and Trp λ_{max} indicate important interactions that induce changes in protein conformation.[86,87] Therefore, in the systems analysed in this study, it was confirmed that the interaction between CALB and AuNPs took place at all concentrations of AuNPs; with significant conformational changes, dependent on the AuNP:CALB ratio. It should be stressed that all inner filter effects regarding the AuNP absorption were corrected, as described in the Experimental section.

Finally, the CALB spectral center of mass (<λ>) was calculated in order to define the degree of protein unfolding with increasing AuNP content. The <λ> is defined by the following weighted average equation:[88]

$$\langle\lambda\rangle = \frac{\sum \lambda_i F_i}{\sum F_i} \quad (6)$$

where, F_i is the fluorescence intensity at λ_i. The <λ> shift was significantly more expressive at higher C_{AuNPs} (Figure 10). Therefore, this means that CALB tertiary structure was partially unfolded at all C_{AuNPs}, this effect being more pronounced with increasing C_{AuNPs}.

In addition, for the sake of comparison, the <λ> of AuNPs@CALB was also determined. It can be observed (red star, Figure 10) that, in this sample, CALB is partially unfolded at this stage. This result can be associated with the Trp λ_{max} fluorescence shift observed in Figure 4a.

Conclusions

In this study, it was demonstrated that CALB can be used as a good stabilizing agent for AuNPs, maintaining its catalytic activity, a key property. In the opposite way, AuNPs also play a role in the stabilization of CALB in aqueous media. Thus, long-term stable bio-hybrid materials, composed of AuNPs and CALB, can be obtained.

Changes in CALB conformational characteristics, as probed by fluorescence and CD spectroscopies, revealed different interaction patterns when comparing $_{SA}$CALB/AuNPs and AuNPs@CALB. The latter exhibits less conformational changes of CALB secondary structure, as observed by CD spectroscopy and further confirmed by the relative catalytic activity. Interestingly, the Trp fluorescence properties of CALB are dependent on the AuNPs concentration. In addition, zeta potential measurements confirmed the higher colloidal stability of AuNPs@CALB.

The in-depth physicochemical investigation presented herein is very useful for future investigations employing enzymes for the stabilization of metallic nanoparticles since bio-functionalities can be inserted into these particles. Likewise, this study contributes to further biocatalysis studies using metallic nanoparticles for enzyme stabilization shedding light on important, but still under-researched, synthetic transformations. The maintenance of the enzymatic activity of both AuNPs@CALB and $_{SA}$CALB/AuNPs demonstrates the potential of these catalytic systems for further application including organic transformations (e.g., kinetic resolution of racemates for which CALB is largely employed). For this, studies involving organic solvent mainly apolar ones must be performed in order to confirm the maintenance of the key properties under non-aqueous conditions.

Finally, the presented results contribute to the development of safer strategies to apply AuNPs in biological media containing enzymes, since the elucidation of the interactions that are taking place at the nano-bio interface provides the basis for the development of new materials with desired biological performance.

Supplementary Information

Supplementary information is available free of charge at http://jbcs.sbq.org.br as PDF file.

Acknowledgments

H. R. B. thanks CAPES (code 001) and M. C. S. thanks CNPq for the scholarships. CAPES, through PROEX program, and CNPq through grant No. 456834/2014-1 are acknowledged for financial support. L. R. S. B. thanks the CNPq research fellowship (308692/2018-7). Many thanks also to the UFPR Electron Microscopy Center (CME-UFPR) and to the Brazilian Nanotechnology National Laboratory (LNNano-CNPEM) for the TEM images. Dr Edileusa C. M. Gerhardt is acknowledged for the help with SEC and SDS-PAGE experiments. MSc Barbara Malheiros, Prof Cristiano L. P. Oliveira and the technician Dennys Reis are acknowledged for the support on the collection of SAXS data in XEUSS instrument. The authors also thank the LNLS staff for SAXS measurements.

References

1. Nel, A. E.; Madler, L.; Velegol, D.; Xia, T.; Hoek, E. M. V.; Somasundaran, P.; Klaessig, F.; Castranova, V.; Thompson, M.; *Nat. Mater.* **2009**, *8*, 543.
2. Huang, R. X.; Lau, B. L. T.; *Biochim. Biophys. Acta, Gen. Subj.* **2016**, *1860*, 945.
3. Wang, J.; Quershi, W. A.; Li, Y. Y.; Xu, J. X.; Nie, G. J.; *Sci. China: Chem.* **2016**, *59*, 1467.
4. Gagner, J. E.; Shrivastava, S.; Qian, X.; Dordick, J. S.; Siegel, R. W.; *J. Phys. Chem. Lett.* **2012**, *3*, 3149.
5. Sun, Y.; Xia, Y.; *Science* **2002**, *298*, 2176.
6. Kohout, C.; Santi, C.; Polito, L.; *Int. J. Mol. Sci.* **2018**, *19*, 3385.
7. Zhao, P. X.; Li, N.; Astruc, D.; *Coord. Chem. Rev.* **2013**, *257*, 638.
8. Alkilany, A. M.; Lohse, S. E.; Murphy, C. J.; *Acc. Chem. Res.* **2013**, *46*, 650.
9. Shankar, S.; Soni, S. K.; Daima, H. K.; Selvakannan, P. R.; Khire, J. M.; Bhargava, S. K.; Bansal, V.; *Phys. Chem. Chem. Phys.* **2015**, *17*, 21517.
10. Shukla, R.; Bansal, V.; Chaudhary, M.; Basu, A.; Bhonde, R. R.; Sastry, M.; *Langmuir* **2005**, *21*, 10644.
11. Niidome, Y.; Haine, A. T.; Niidome, T.; *Chem. Lett.* **2016**, *45*, 488.
12. Harrison, E.; Hamilton, J. W. J.; Macias-Montero, M.; Dixon, D.; *Nanotechnology* **2017**, *28*, 295602.
13. Maruyama, T.; Fujimoto, Y.; Maekawa, T.; *J. Colloid Interface Sci.* **2015**, *447*, 254.
14. Chan, K. P.; Gao, Y.; Goh, J. X. W.; Susanti, D.; Yeo, E. L. L.; Chao, S. H.; Kah, J. C. Y.; *ACS Appl. Mater. Interfaces* **2017**, *9*, 10408.
15. Baumann, V.; Muhammed, M. A. H.; Blanch, A. J.; Dey, P.; Rodriguez-Fernandez, J.; *Isr. J. Chem.* **2016**, *56*, 195.
16. Yang, T.; Li, Z.; Wang, L.; Guo, C. L.; Sun, Y. J.; *Langmuir* **2007**, *23*, 10533.
17. Alex, S. A.; Chakraborty, D.; Chandrasekaran, N.; Mukherjee, A.; *RSC Adv.* **2016**, *6*, 52683.
18. Wang, G. K.; Liu, X. B.; Yan, C. L.; Bai, G. Y.; Lu, Y.; *Colloids Surf., B* **2015**, *135*, 261.
19. Lv, M.; Zhu, E. G.; Su, Y. Y.; Li, Q. N.; Li, W. X.; Zhao, Y.; Huang, Q.; *Prep. Biochem. Biotechnol.* **2009**, *39*, 429.
20. Ravikumar, S.; Sreekanth, T. V. M.; Eom, I. Y.; *J. Nanosci. Nanotechnol.* **2015**, *15*, 9617.
21. Kisukuri, C. M.; Macedo, A.; Oliveira, C. C. S.; Camargo, P. H. C.; Andrade, L. H.; *Langmuir* **2013**, *29*, 15974.
22. Mala, J. G. S.; Takeuchi, S.; *Anal. Chem. Insights* **2008**, *3*, 9.
23. Ge, J.; Lu, D. A.; Wang, J.; Liu, Z.; *Biomacromolecules* **2009**, *10*, 1612.
24. Johnson, B. J.; Algar, W. R.; Malanoski, A. P.; Ancona, M. G.; Medintz, I. L.; *Nano Today* **2014**, *9*, 102.
25. Albarrán-Velo, J.; González-Martínez, D.; Gotor-Fernández, V.; *Biocatal. Biotransform.* **2018**, *36*, 102.
26. Chapman, J.; Ismail, A. E.; Dinu, C. Z.; *Catalysts* **2018**, *8*, 238.
27. Sheldon, R. A.; Brady, D.; *Chem. Commun.* **2018**, *54*, 6088.
28. Hughes, D. L.; *Org. Process Res. Dev.* **2018**, *22*, 1063.
29. Rabbani, G.; Ahmad, E.; Khan, M. V.; Ashraf, M. T.; Bhat, R.; Khan, R. H.; *RSC Adv.* **2015**, *5*, 20115.
30. Wu, Q.; Soni, P.; Reetz, M. T.; *J. Am. Chem. Soc.* **2013**, *135*, 1872.
31. Zhan, Z.; Di, L.; Zhang, X.; Li, Y.; *Plasma Sci. Technol.* **2016**, *18*, 494.
32. Anderson, E. M.; Larsson, K. M.; Kirk, O.; *Biocatal. Biotransform.* **1998**, *16*, 181.
33. Kirk, O.; Borchert, T. V.; Fuglsang, C. C.; *Curr. Opin. Biotechnol.* **2002**, *13*, 345.
34. Kirk, O.; Christensen, W. M.; *Org. Process Res. Dev.* **2002**, *6*, 446.
35. Gotor-Fernández, V.; Busto, E.; Gotor, V.; *Adv. Synth. Catal.* **2006**, *348*, 797.
36. Zhang, Q.; Lima, D. Q.; Lee, I.; Zaera, F.; Chi, M.; Yin, Y.; *Angew. Chem., Int. Ed.* **2011**, *50*, 7088.
37. Lima, R. N.; dos Anjos, C. J.; Orozco, E. V. M.; Porto, A. L. M.; *Mol. Catal.* **2019**, *466*, 75.
38. Ansari, S. A.; Husain, Q.; *Biotechnol. Adv.* **2012**, *30*, 512.
39. Laszlo, J. A.; Evans, K. O.; *J. Mol. Catal. B: Enzym.* **2007**, *48*, 84.
40. Zisis, T.; Freddolino, P. L.; Turunen, P.; van Teeseing, M. C. F.; Rowan, A. E.; Blank, K. G.; *Biochemistry* **2015**, *54*, 5969.

41. Palomo, J. M.; Fernandez-Lorente, G.; Mateo, C.; Fuentes, M.; Fernandez-Lafuente, R.; Guisan, J. M.; *Tetrahedron: Asymmetry* **2002**, *13*, 1337.
42. Fernandez-Lorente, G.; Cabrera, Z.; Godoy, C.; Fernandez-Lafuente, R.; Palomo, J. M.; Guisan, J. M.; *Process Biochem.* **2008**, *43*, 1061.
43. Cabrera, Z.; Fernandez-Lorente, G.; Fernandez-Lafuente, R.; Palomo, J. M.; Guisan, J. M.; *J. Mol. Catal. B: Enzym.* **2009**, *57*, 171.
44. Wu, J. M.; Li, X.; Yan, Y. E.; Hu, Y. Y.; Zhang, Y. H.; Tang, Y.; *J. Colloid Interface Sci.* **2013**, *406*, 130.
45. Moghadam, T. T.; Ranjbar, B.; Khajeh, K.; Etezad, S. M.; Khalifeh, K.; Ganjalikhany, M. R.; *Int. J. Biol. Macromol.* **2011**, *49*, 629.
46. Venditti, I.; Palocci, C.; Chronopoulou, L.; Fratoddi, I.; Fontana, L.; Diociaiuti, M.; Russo, M. V.; *Colloids Surf., B* **2015**, *131*, 93.
47. Tang, Y.; Zhang, W.; Liu, J.; Zhang, L.; Huang, W.; Huo, F. W.; Tian, D. B.; *Nanoscale* **2015**, *7*, 6039.
48. Kisukuri, C. M.; Palmeira, D. J.; Rodrigues, T. S.; Camargo, P. H. C.; Andrade, L. H.; *ChemCatChem* **2016**, *8*, 171.
49. Wu, C. S.; Wu, C. T.; Yang, Y. S.; Ko, F. H.; *Chem. Commun.* **2008**, 5327.
50. Bradford, M. M.; *Anal. Biochem.* **1976**, *72*, 248.
51. Piella, J.; Bastús, N. G.; Puntes, V.; *Chem. Mater.* **2016**, *28*, 1066.
52. de Barros, H. R.; Cardoso, M. B.; de Oliveira, C. C.; Franco, C. R. C.; Belan, D. D.; Vidotti, M.; Riegel-Vidotti, I. C.; *RSC Adv.* **2016**, *6*, 9411.
53. http://imagej.net, accessed in May 2019.
54. Lukach, A.; Therien-Aubin, H.; Querejeta-Fernandez, A.; Pitch, N.; Chauve, G.; Methot, M.; Bouchard, J.; Kumacheva, E.; *Langmuir* **2015**, *31*, 5033.
55. Lakowicz, J. R.; *Principles of Fluorescence Spectroscopy*; Kluwer Academic: New York, 1999.
56. Rabbani, G.; Ahmad, E.; Khan, M. V.; Ashraf, M. T.; Bhat, R.; Khan, R. H.; *RSC Adv.* **2015**, *5*, 20115.
57. de Castro, C. E.; Mattei, B.; Riske, K. A.; Jager, E.; Jager, A.; Stepanek, P.; Giacomelli, F. C.; *Langmuir* **2014**, *30*, 9770.
58. Guinier, A.; Fournet, G.; *Small-Angle Scattering of X-Rays*; Wiley: New York, 1955.
59. Glatter, O.; Kratky, O.; *Small-Angle X-Ray Scattering*; Academic Press Inc.: London, 1982.
60. Bergmann, A.; Fritz, G.; Glatter, O.; *J. Appl. Crystallogr.* **2000**, *33*, 1212.
61. Torres-Bugeau, C. M.; Avila, C. L.; Raisman-Vozari, R.; Papy-Garcia, D.; Itri, R.; Barbosa, L. R. S.; Cortez, L. M.; Sim, V. L.; Chehin, R. N.; *J. Biol. Chem.* **2012**, *287*, 2398.
62. Lima, V. M. G.; Krieger, N.; Mitchell, D. A.; Fontana, J. D.; *Biochem. Eng. J.* **2004**, *18*, 65.
63. Daniel, M. C.; Astruc, D.; *Chem. Rev.* **2004**, *104*, 293.
64. Turkevich, J.; Stevenson, P. C.; Hillier, J.; *Discuss. Faraday Soc.* **1951**, *11*, 55.
65. Roduner, E.; *Chem. Soc. Rev.* **2006**, *35*, 583.
66. Liz-Marzan, L. M.; *Mater. Today* **2004**, *7*, 26.
67. Kelly, K. L.; Coronado, E.; Zhao, L. L.; Schatz, G. C.; *J. Phys. Chem. B* **2003**, *107*, 668.
68. Yu, J.; Becker, M. L.; Carri, G. A.; *Langmuir* **2012**, *28*, 1408.
69. Rabbani, G.; Ahmad, E.; Zaidi, N.; Fatima, S.; Khan, R. H.; *Cell Biochem. Biophys.* **2012**, *62*, 487.
70. Venugopal, A.; Kumar, C. S.; Kumar, N. S.; Swamy, M. J.; *Int. J. Biol. Macromol.* **2017**, *104*, 432.
71. Ito, A.; Berardi, M.; Pazin, W.; *Fluorescência e Aplicações em Biofísica*; Editora da Física: São Paulo, Brasil, 2016.
72. Kelly, S. M.; Jess, T. J.; Price, N. C.; *Biochim. Biophys. Acta, Proteins Proteomics* **2005**, *1751*, 119.
73. Greenfield, N. J.; Fasman, G. D.; *Biochemistry* **1969**, *8*, 4108.
74. Clayden, J.; Greeves, N. J.; Warren, S.; *Organic Chemistry*; Oxford University Press: Oxford, 2012.
75. Altman, D. G.; Bland, J. M.; *BMJ* **2005**, *331*, 903.
76. Schultz, N.; Metreveli, G.; Franzreb, M.; Frimmel, F. H.; Syldatk, C.; *Colloids Surf., B* **2008**, *66*, 39.
77. Aghili, Z.; Taheri, S.; Zeinabad, H. A.; Pishkar, L.; Saboury, A. A.; Rahimi, A.; Falahati, M.; *PLoS One* **2016**, *11*, e0164878.
78. Schollbach, M.; Zhang, F.; Roosen-Runge, F.; Skoda, M. W. A.; Jacobs, R. M. J.; Schreiber, F.; *J. Colloid Interface Sci.* **2014**, *426*, 31.
79. Feng, T.; Chen, Y.; Feng, B. B.; Yan, J. L.; Di, J. W.; *Spectrochim. Acta, Part A* **2019**, *206*, 97.
80. Tsogas, G. Z.; Kappi, F. A.; Vlessidis, A. G.; Giokas, D. L.; *Anal. Lett.* **2018**, *51*, 443.
81. Sasaki, Y. C.; Yasuda, K.; Suzuki, Y.; Ishibashi, T.; Satoh, I.; Fujiki, Y.; Ishiwata, S.; *Biophys. J.* **1997**, *72*, 1842.
82. Maji, A.; Beg, M.; Mandal, A. K.; Das, S.; Jha, P. K.; Kumar, A.; Sarwar, S.; Hossain, M.; Chakrabarti, P.; *J. Mol. Struct.* **2017**, *1141*, 584.
83. Irani, M.; Tornvall, U.; Genheden, S.; Larsen, M. W.; Hatti-Kaul, R.; Ryde, U.; *Biochemistry* **2013**, *52*, 1280.
84. Emer, M.; Cardoso, M. B.; *J. Mater. Chem. B* **2017**, *5*, 8052.
85. Momeni, L.; Shareghi, B.; Saboury, A. A.; Farhadian, S.; Reisi, F.; *Int. J. Biol. Macromol.* **2017**, *94*, 145.
86. Dantas, M. D. D.; Tenorio, H. D.; Lopes, T. I. B.; Pereira, H. J. V.; Marsaioli, A. J.; Figueiredo, I. M.; Santos, J. C. C.; *Int. J. Biol. Macromol.* **2017**, *102*, 505.
87. Tang, L.; Li, S.; Bi, H. N.; Gao, X.; *Food Chem.* **2016**, *196*, 550.
88. Mohana-Borges, R.; Silva, J. L.; de Prat-Gay, G.; *J. Biol. Chem.* **1999**, *274*, 7732.

Submitted: February 1, 2019
Published online: June 6, 2019